PENSOFT

SENCKENBERG
world of biodiversity

Leibniz Association

Osteology of the caecilian *Gegeneophis carnosus* (Beddome, 1870) (Amphibia: Gymnophiona: Grandisoniidae) from the Western Ghats of peninsular India

Shamna Rajan Palakkool[1], David J. Gower[1,2], Ramachandran Kotharambath[1,2]

1 *Department of Zoology, Central University of Kerala, Tejaswini Hills, Periya, Kasaragod, Kerala, India*

2 *Department of Life Sciences, Natural History Museum, London, SW7 5BD, UK*

http://zoobank.org/6F2CD8C3-952C-45E1-B33A-FDFD47ED0E44

Corresponding authors: Shamna Rajan Palakkool (shamnarajan42@gmail.com); Ramachandran Kotharambath (ramachandrank6@gmail.com)

Academic editor Raffael Ernst | **Received** 29 December 2021 | **Accepted** 16 June 2022 | **Published** 20 July 2022

Citation: Palakkool SR, Gower DJ, Kotharambath R (2022) Osteology of the caecilian *Gegeneophis carnosus* (Beddome, 1870) (Amphibia: Gymnophiona: Grandisoniidae) from the Western Ghats of peninsular India. Vertebrate Zoology 72 561–576. https://doi.org/10.3897/vz.72.e79911

Abstract

The osteology of the poorly known grandisoniid caecilian *Gegeneophis carnosus* is described for the first time by applying high-resolution X-ray micro-computed tomography to some recently collected material. The ossified skeleton comprises a stegokrotaphic skull, lower jaw, and vertebral column. The braincase, composed of the sphenethmoid and os basale, is covered by eight other cranial elements viz. nasopremaxilla, frontal, parietal, squamosal, pterygoquadrate, maxillopalatine, vomer, and stapes. The eye is covered by the maxillopalatine, and an (open) orbit is absent. The sphenethmoid is not exposed and lacks a solum nasi or a ventral flange. The olfactory chamber lacks an olfactory eminence. Slight asymmetries were observed in the structure and/or size of the left and right frontals and parietals and in the number and size of some foramina. Except for pterygoquadrate and stapes, all bones are pierced by foramina for nerves and/or blood vessels. The lower jaw shows a typical caecilian pattern with dentigerous pseudodentary and edentulous pseudoangular. Numbers of vertebrae range from 123–130 (mean 126). The vertebrae are somewhat heterogenous, varying in size and proportions along the column. Comparisons are made with other caecilians, especially other grandisoniids. Aspects of the cranial osteology of *Gegeneophis*, such as the closed orbit, subterminal mouth, and stegokrotaphy are possible adaptations to dedicated fossoriality, but functional, behavioural, and field ecological data are not yet available to test this.

Keywords

Cranium, lower jaw, mandible, micro-CT, skeleton, skull, stegokrotaphy, vertebrae

Introduction

Gegeneophis Peters, 1880 is a genus of soil-burrowing caecilians endemic to the Western and Eastern Ghats of peninsular India. Caecilians (Gymnophiona) lack limbs and limb girdles, and most species burrow in soils, at least as adults. The ossified skeletal systems of adult caecilians comprise a robust skull, lower jaw, and a flexible vertebral column with a short or absent tail (Taylor 1968; Wake 2003; Carroll 2007; Vitt and Caldwell 2014). The advent of high-resolution X-ray Micro Computed Tomography (μCT) has advanced the non-destructive exploration of

details of caecilian skeletal anatomy (e.g., Wilkinson et al. 2011; Maddin et al. 2012; Sherratt et al. 2014), providing an excellent complementary tool alongside more traditional methods such as clearing and staining, histology, and maceration and drying (see Ramaswami 1942; Taylor 1969; Wake 1980; Müller et al. 2005). In general, the caecilian skull has been modified for head-first burrowing in soil, with variation in fenestration, shape, and composition of elements across the families that is only partly understood (Taylor 1969; Nussbaum 1977; Wake 2003; Carroll 2007; Sherratt et al. 2014; Bardua et al. 2019). Compared to more surface-active caecilians, the crania of *Gegeneophis* spp. studied thus far are more heavily constructed and have fewer ossified elements (e.g., Taylor 1969; Duellman and Trueb 1986; Wake 2003).

Current knowledge of *Gegeneophis* skeletal morphology is based mostly on studies of *G. ramaswamii* (see Ramaswami 1942, 1947; Taylor 1969, 1977a, 1977b; Müller et al. 2005; Maddin 2011; Maddin et al. 2012). Additionally, Sherratt et al. (2014) and Bardua et al. (2019) included specimens of *G. carnosus* in their quantitative studies of the evolution of shape and modularity of caecilian skulls. Specimens of *G. carnosus* reported from localities in the far southern end of the range of the genus studied by Ramaswami (1942, 1947) might instead be *G. ramaswamii*, because that is the only *Gegeneophis* species known to occur south of the Palghat Gap based on verified, vouchered records (e.g., Gower et al. 2004a; Gower et al. 2011). The likely erroneously identified specimens were collected from Pujapura near Trivandrum (Ramaswami 1942) and Tenmalai near Kollam (Ramaswami 1947); Tenmalai is the type locality of the subsequently described *G. ramaswamii* (Taylor 1964). *Gegeneophis carnosus* is known with certainty only from the vicinity of its type locality at Peria, at an elevation of approximately 1,000–1,500 m in the Wayanad district of north Kerala.

Here we present the first detailed documentation of the skeletal anatomy of *G. carnosus* based on newly generated μCT data. We make comparisons with available data for other members of Grandisoniidae, and especially with the only congener for which skeletal anatomy has been described in any detail, *G. ramaswamii.*

Materials and Methods

Specimens

Nine specimens of *G. carnosus* were collected from the vicinity of its type locality Peria, Wayanad, on 14th July 2015 by Ramachandran Kotharambath and colleagues. The specimens were lethally anaesthetised using MS222 solution followed by fixation in 4–6% formalin for 48 hours and preservation in 70% alcohol. The specimens ranged from 112–209 mm in total length, and all are female, based on observation of ova via incisions into the coelom. Specimens are currently stored in the Department of Zoology of Central University Kerala with field tags RAM 0020, 0023, 0031, 0033, 0035, 0044, 0045, 0047, 0049. The specimen subjected to the μCT technique, RAM 0020, has a preserved total length of 198 mm, and a maximum skull length of approximately 4.8 mm. All nine specimens were subjected to two-dimensional (2D) radiography to count vertebrae. We followed Dubois et al. (2021) family-level classification, and most other recent studies instead applied the name Indotyphlidae to the family containing *Gegeneophis* (e.g. Wilkinson et al. 2011).

Micro-computed tomography

The specimen was subjected to high-resolution X-ray μCT scanning (Bruker SkyScan 1272, 20 to 100 kV, 10 W) at the Centre for Cellular and Molecular Platform (C-CAMP), National Centre for Biological Sciences (NCBS), Bengaluru, Karnataka, India. The specimen was folded and mounted in a tube, without ethanol, and Styrofoam balls were added to prevent movement during rotation. The scan was conducted in 180˚, with rotation steps of 0.8˚ (i.e., 225 projections) for 20 min 12 s with an exposure of 1452 ms and an image resolution of 3.1 μm. The source voltage was 45 kV with a source current of 220 μA. The scanned images were reconstructed using NRecon 1.7.1.6 (Bruker μCT, Kontich, Belgium) with a voxel size of 3.1 μm. Visualisation of the 3D morphology of the skull and vertebrae was undertaken with CTvox 3.3.0.0 (Bruker μCT, Kontich, Belgium). The 3D model of the μCT dataset was constructed using CT Analyser Version: 1.18.8.0 (Bruker μCT, Kontich, Belgium), and the model was analysed using MeshLab v2020.06 for Windows 64 bits version. The description includes only the ossified structures because the μCT scan data did not permit faithful rendering of cartilaginous structures. The third and fourth vertebrae are excluded from the figures because scan data were obtained only for the anteriormost, midbody, and posteriormost vertebrae.

2D radiography

The specimens were radiographed with an X-ray machine (Wipro GE 300 mA) at Krishna Medical Centre, Kanhangad, Kasaragod, Kerala. Vertebrae were counted on radiographs under a binocular stereoscopic microscope (Olympus SZ61) using a pin.

Terminology and the identification of foramina

We followed Ramaswami (1941, ’42), Müller et al. (2005), and Maddin et al. (2012) for the terminology of skull elements and their parts, and followed Norris and Hughes (1918), Ramaswami (1941), Maddin (2011), and Maddin et al. (2012) for identifying cranial foramina. For the lower jaw, we followed Norris and Hughes (1918), Ramaswami (1941, 1942), Wake and Hanken

(1982), Wilkinson and Nussbaum (1997), Müller (2006), and Maddin (2011), and for vertebrae, we followed Wake (1980), Wilkinson (1992), and Lowie et al. (2022).

List of abbreviations

ac – atlantal cotyle
ae – anterolateral expansion of sphenethmoid
af – alveolar foramen
afp – articular facet for pseudoangular on pterygoquadrate
aot – anterior opening of tentacular canal
aps – anterior process on stapes
aw – antotic wall
ba – basicranial articulation of os basale
bp – basal process of pterygoquadrate
c – centrum
ca – capitulum
cc – concavity holding the Choanenschleimbeutal on maxillopalatine
ch – choana
cp – columellar process
cpr – canalis primordialis
d – dentary tooth row
dch – depression for cerebral hemisphere
dh – depression for hypophysis
dlw – dorsal facet of lateral wall of sphenethmoid
dns – dorsal facet of nasal septum
dp – dorsomedial process of sphenethmoid
dpp – diapophysis
ds – dorsal surface of otic occipital complex of os basale
dv – depression for vomeronasal organ on maxillopalatine
dvv – depression on the vomer continuous with dv on maxillopalatine
en – external naris
f – frontal
fca – foramen for carotid artery
fdf – foramen for 'dorsal fifth' nerve (sensory nerve from the dorsal branch of the trigeminal nerve)
fdv – foramen for dorsal vein
fe – endolymphatic foramen
ff – facet for the frontal on parietal
fI$_d$ – foramen for dorsal branch of the olfactory nerve
fII – foramen for the optic nerve
fI$_v$ – foramen for ventral branch of the olfactory nerve
fj – jugular foramen
fm – foramen magnum
fmp – facet for the maxillopalatine on squamosal
fn – facet for the nasopremaxilla on frontal
fo – fenestra ovalis
fp – perilymphatic foramen
fpa – facet for the processus ascendence on squamosal
fpd – facet overlapped by the pseudodentary on pseudoangular
fpp – facet overlapped by the pseudoangular on pseudodentary
fpq – facet for pterygoquadrate on os basale
fps – facet for the parietal on squamosal
fri – foramen for the intermandibular branch of the trigeminal nerve
fsn – foramina for spinal nerve
ft – foramen transmitting the tentacular (nasolacrimal) duct
fVII – foramen for the facial nerve
fVIII$_a$ – foramen for anterior branch of the vestibulocochlear nerve
fVIII$_m$ – foramen for medial branch of the vestibulocochlear nerve
fVIII$_p$ – foramen for posterior branch of the vestibulocochlear nerve
fV$_{md}$ – foramen for the mandibular division of the trigeminal nerve
fV$_{md}$, ma – foramen for the mandibular division of the trigeminal nerve and mandibular artery
fV$_{mxl}$ – foramen for lateral branch of the maxillary division of the trigeminal nerve
fV$_{mxm}$ – foramen for medial branch of the maxillary division of the trigeminal nerve
fV$_{op}$ – foramen for the ophthalmic division of the trigeminal nerve
fV$_{op,mx,md}$ – foramen for ophthalmic, maxillary and mandibular divisions of the trigeminal nerve
fV$_{opv}$ – foramen for ventral branch of the ophthalmic division of the trigeminal nerve
fvv – foramen for the ventral vein
hy– hypapophysis
i – inner mandibular tooth
lb – labial row of teeth on maxillopalatine
lf – lateral facet of parietal
lg– lingual row of teeth on maxillopalatine
m – meckelian bone
mc – mandibular cotyle
mp – maxillopalatine
mpc – mediopalatinal cavity
na – neural arch
np – nasopremaxilla
nr – nuchal ridge
ns – nasal septum
ob – os basale
oc – occipital condyle
p – parietal
pa – pseudoangular
pas – processus ascendens of pterygoquadrate
pc – processus condyloideus of pseudoangular
pd –pseudodentary
pf – facet for parietal on os basale
pi – processus internus of pseudoangular
po – processus oticus
poc – petro-occipital cavity
poz – postzygapophysis
pp – premaxillary process
pq – pterygoquadrate
pr – parasphenoid rostrum
prp – parapophysis
prz – prezygapophysis
ps – parasphene
r – rib
rp – retroarticular process

rv – ridge on vomer
s – squamosal
sph – sphenethmoid
sr – 'splenial' ridge
srf – spinal root foramen
st – stapes
sv – sulcus on vomer
t – tuberculum
tc – tentacular canal
tr – transverse ridge on maxillopalatine between the dv and cc
v – vomer
vf – vomerine foramen
vk – ventral keel
vns – ventral facet of nasal septum
wp – wing-like projection ventral to the otic capsule

Results

Skull

Ten ossified cranial elements constitute the stegokrotaphic skull. The neurocranium is composed of sphenethmoid and os basale and is partly encased by the nasopremaxillae, frontals, parietals, maxillopalatines, squamosals, vomers, pterygoquadrates, and stapes (Figs 1A–C, 2A–C). The skull is bullet-shaped, with its minimum width at its apex and maximum width at the region where the squamosal overlies the pterygoquadrate (Fig. 1A–C). The anterior tip of the mouth is subterminal, lying beneath a somewhat projecting snout tip. The dorsal portion of the nasopremaxillae, frontals, and parietals form the major skull roofing. The posteriormost part of the roof is constituted by the dorsal surface of the otic-occipital complex of the os basale, which is the only contribution of the neurocranium to the skull roof (Fig. 1A). Dorsally, a narrow median fissure divides the skull roof into two more or less symmetrical halves. In lateral view, the skull is formed by the lateral side of the nasopremaxilla, and maxillopalatine, squamosal, quadrate part of the pterygoquadrate, the lateral side of the otic-occipital complex of the os basale, and stapes (Fig. 1B). The anterior half of the ventral portion of the skull covering the sphenethmoid is occupied by the premaxillary parts of the nasopremaxillae, vomers, and palatine shelves of the maxillopalatines. The posterior half is constituted mainly by the os basale, and the pterygoquadrates forms the remaining part on either side (Fig. 1C).

The eyes are small and covered by maxillopalatines, and so orbits are absent (closed). The seven major external openings are the foramen magnum and the paired external nares, openings of the tentacular canals, and choanae (Figs 1A–C, 2F). The subcircular external naris is large and bordered by nasopremaxilla (Fig. 1B). The choana has an oval cross section and communicates between the dorsal and ventral surfaces of the palate in an anterodorsal (and slightly lateral) to posteroventral (and slightly medial) trajectory. The choana is bordered mainly by palatine and slightly by vomer (Fig. 1C). The tentacular canal opening lies at the anterior extremity of the maxillopalatine, directed anteriorly and slightly laterally (Fig. 1A, B). The tentacular canal is enclosed by the maxillopalatine (Figs 1B, 3J, L, M). The foramen magnum is dorsally arched with a narrow base and bordered by os basale (Fig. 2F). In ventral view, two incompletely separated cavities lie between the pterygoquadrate and the os basale, the mediopalatinal and the petro-occipital cavities (*sensu* Nussbaum 1977, 1979) (Fig. 1C).

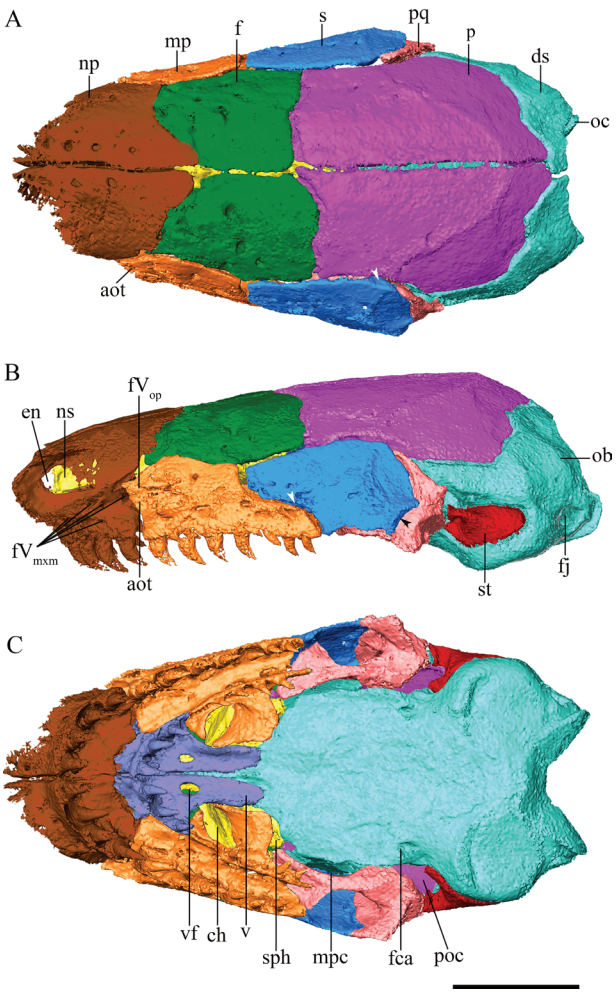

Figure 1. The skull of *Gegeneophis carnosus* (RAM 0020). **A** dorsal view (arrowhead indicates the facet for the parietal on the squamosal; **B** lateral view (white arrowhead indicates the lateral facet for the maxillopalatine; black arrowhead indicates the lateral facet for the pterygoquadrate on the squamosal); **C** ventral view. Scale bar: 1mm.

Sphenethmoid

The anterior of the braincase is constituted by the compound sphenethmoid. It has a main body, from which arises an anteriorly projecting long slender nasal septum and a posteriorly projecting, slightly shorter but broader dorsomedial process (mesethmoid). The lateral wall of the main body has a very short anterior expansion (Fig. 2A–C). The sphenethmoid lacks a solum nasi and a lat-

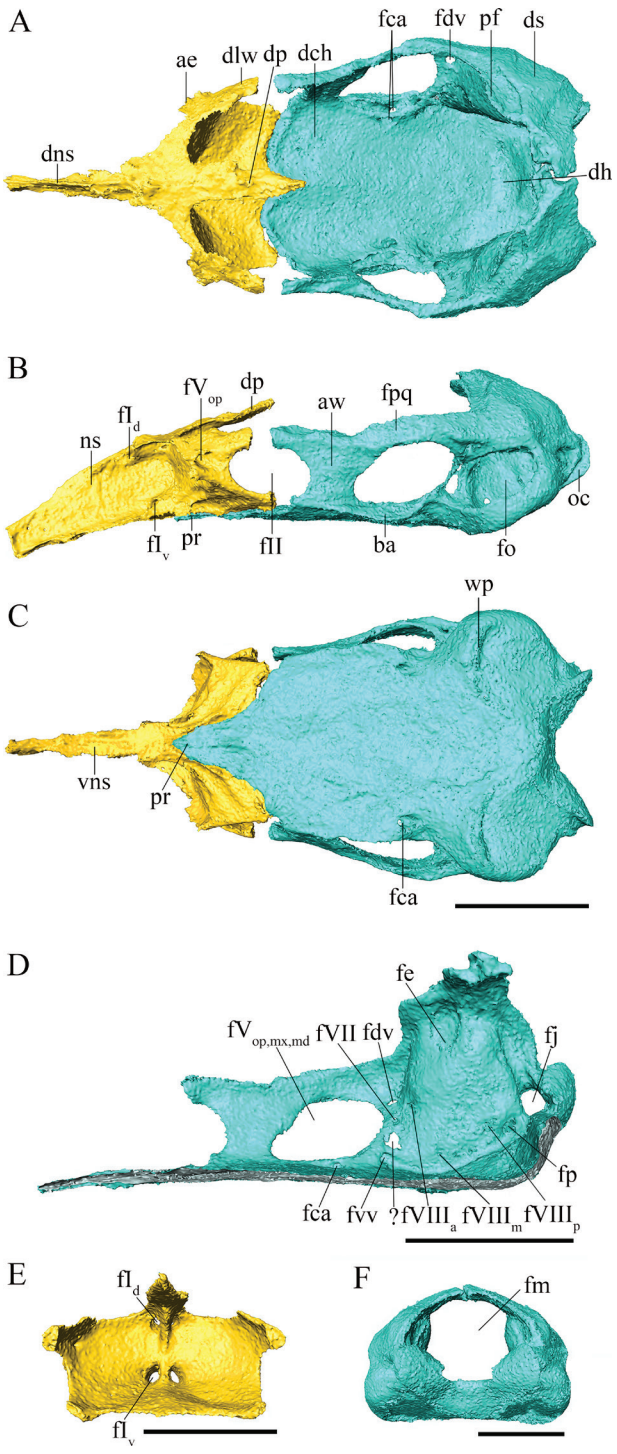

Figure 2. The braincase of *Gegeneophis carnosus* (RAM 0020). **A** dorsal view; **B** lateral view; **C** ventral view; **D** right medial surface of the os basale; **E** posterior view of the sphenethmoid; **F** posterior view of the os basale. Scale bars: 1 mm.

erally projecting ventral flange (present in some other caecilians: Maddin et al. 2012). The main body constitutes less than 30% of the element's total length. In dorsal view, the posterior margin of the ventral surface is concave on either side of the midline (Fig. 2A). The anterior wall of the sphenethmoid is perforated by two bilateral pairs of foramina for dorsal and ventral branches of the olfactory nerves. Both pairs of foramina lie close to the midline (Fig. 2E).

After passing through the anterior wall of the element, the passage of the dorsal and ventral branches of the olfactory nerve opens at the foramina at the base of the nasal septum (Fig. 2B). The foramen for the ophthalmic division of the trigeminal nerve pierces the anterolateral corner (Fig. 2B). Posterior to the anterolateral expansion lies the moderately broad dorsal facet of the lateral wall (Fig. 2A). The posterior margin of the lateral wall is deeply incised by the anterior margin of the optic foramen (Fig. 2B). The nasal septum accounts for 50% or more of the total length of the sphenethmoid. Its dorsal facet is broad at its base; it narrows gradually for a short distance and becomes thin and blade-like (Fig. 2A). The ventral facet narrows anteriorly and is broader than the dorsal facet (Fig. 2C). The nasal septum slightly tapers anteriorly in lateral view (Fig. 2B). Posterior to the nasal septum lies the dorsomedial process with an acute posterior terminus, lying just beneath the parietals. This process is broader than the dorsal facet of the nasal septum and the lateral wall of the sphenethmoid (Fig. 2A).

Os basale

The compound os basale lies immediately behind (and articulates with) the sphenethmoid and constitutes the major part of the braincase (Fig. 2A). The parasphenoid rostrum extends anteriorly up to the base of the nasal septum (Fig. 2B, C). Posterior to the rostrum, two large, shallow depressions are present on the dorsal surface, housing the cerebral hemispheres (Fig. 2A). The antotic walls (pleurosphenoid portion) lie lateral to these depressions (Fig. 2A, B). The anterior margin of each antotic wall is deeply incised by the posterior margin of the optic foramen (Fig. 2B). The dorsal facet of the antotic wall is slightly narrower than that of the lateral wall of the sphenethmoid (Fig. 2A). Another prominent depression is present on the posterior of the floor of the endocranial cavity, which houses the hypophysis of the brain (Fig. 2A).

A large foramen, transmitting the ophthalmic, maxillary, and mandibular divisions of the trigeminal nerve, occupies most of the antotic wall (Fig. 2D). Dorsal to it lies the poorly demarcated articular facet for the pterygoquadrate (Fig. 2B). The foramina for the passage of the dorsal vein, facial nerve, and ventral vein lie posterodorsal, posteromedial, and posteroventral to the large foramen, respectively (Fig. 2D). A void (?, Fig. 2D) is present between the foramina for the facial nerve and ventral vein, encompassing part of the anterior process of the stapes. The foramen for the anterior branch of the vestibulocochlear nerve lies posteroventral and posterodorsal to the foramina interpreted as for the dorsal vein and the facial nerve, respectively (Fig. 2D). The foramen on the interior of the dorsal surface of the otic-occipital complex transmits the endolymphatic duct (Fig. 2D).

The ceiling of the otic capsule has three interconnected chambers. The foramina for the perilymphatic duct and the posterior branch of the vestibulocochlear nerve lie along the median wall of the otic capsule immediately above the floor (Fig. 2D). Anterior to these foramina lies

a tiny foramen, likely for the passage of the medial branch of the vestibulocochlear nerve (Fig. 2D). The foramen for the medial branch of the vestibulocochlear nerve on the medial wall of the left otic capsule is larger than that on the right. The elliptical fenestra ovalis is located on the lateral wall of the otic-occipital complex, posterior to the large foramen transmitting the ophthalmic, maxillary, and mandibular divisions of the trigeminal nerve (Fig. 2B). The incision of the lateral wall of the otic-occipital complex by the fenestra ovalis is negligible in the posterior view of the os basale (Fig. 2F). The jugular foramen is posterior to the fenestra ovalis and anterior to the occipital condyle and is approximately as large as the anterior opening of the tentacular canal (Figs 1B, 2B, D).

The occipital condyle projects back beyond the posterior limit of the otic capsule (Figs 1B, 2B). The basicranial articulation is ventrolateral to the antotic wall and is slightly tilted ventrally (Fig. 2B). The foramen for the entrance of the carotid artery into the braincase lies immediately posteroventral to the basicranial articulation (Fig. 2C). The bony channel for the artery bifurcates, with a pair of foramina on each side of the braincase, each member of the pair separated by a narrow ridge on the endocranial floor, close to the lower margin of the large foramen (Fig. 2A, D). The wing-like projection ventral to the otic capsule is not prominent (Fig. 2C). Dorsally, the os basale bears an undulating facet for articulation with the parietal (Fig. 2A).

Nasopremaxilla

The nasopremaxilla of caecilians is a compound, dentigerous bone formed by the fusion of nasal, premaxilla, and septomaxilla, with an internal cavity that houses the olfactory sac and vomeronasal organ (Ramaswami 1942; Wake 2003; Müller et al. 2005). In *G. carnosus*, it is longer dorsally than ventrally, has a somewhat sinusoidal posterior edge both dorsally and ventrally, and attains maximum width between the external nares and the region contact with the anterior of the maxillopalatine posterolaterally (Fig. 1A, C). Each nasopremaxilla bears four teeth on the premaxillary labial row, plus one replacement tooth on the right and two on the left nasopremaxilla (Fig. 1C); these smaller replacement teeth are closely associated with the lingual surface of the base of corresponding larger, functional teeth. The nasal septum of the sphenethmoid occupies the space between the two nasopremaxillae (Fig. 1B). The internal surface of each nasal part of the nasopremaxillae bears a foramen close to the median fissure for passage of the ophthalmic division of the trigeminal nerve, which exits the neurocranium via the anterolateral corner of the sphenethmoid (Fig. 3A). The foramen leads to a channel that opens directly to the tip of the nasopremaxilla and has four and five openings on the left and right bones, respectively, on the dorsal surface.

A depression on the medial floor of the nasopremaxilla accommodates the premaxillary process of the vomer. A medial foramen found in this depression ventral to the ventral facet of the nasal septum (Fig. 3A) is presumed to transmit the ventral branch of the ophthalmic division of the trigeminal nerve. The passage of the medial branch of the maxillary division of the trigeminal nerve is correlated with a closed channel and several foramina present on the lateral surface of the element, slightly above the dental margin and anterior to the opening of the tentacular canal (Figs 1B, 3A).

Frontal

The frontal lies posterior to the nasopremaxilla with which it shares a tight sutural contact. The frontal also contacts the parietal posteriorly, the maxillopalatine anteroventrally, and the squamosal posteroventrally (Fig. 1A, B). The frontals are slightly longer than wide, with the greatest width approximately at mid-length. The left frontal is slightly longer than the right and has a much larger facet for articulation with the nasopremaxilla anterodorsally (Fig. 3B). The dorsal surface of each frontal bears seven foramina (Fig. 3B), presumed to be for branchlets of the ophthalmic division of the trigeminal nerve. The passage of one branchlet of the ophthalmic division of the trigeminal nerve between the sphenethmoid and nasopremaxilla correlates with a shallow canal on the ventral surface (white arrowheads in Fig. 3C). Beside this canal lies one or two narrow, shallow grooves for another branchlet of the ophthalmic division of the trigeminal nerve; these grooves communicate with the foramina lying on the anterodorsal edge of the bone (black arrowheads in Fig. 3B, C).

Parietal

The parietal, the largest bone in the dermatocranium, is longer than wide. In dorsal view, it is widest at the level with the posterior of the pterygoquadrate (Fig.1A). Anteriorly, the dorsal surface of the element has a facet (larger on the left) for the overlying frontal (Fig. 3D). Posteriorly, the edges of the element are irregular and overlay the facet for the parietal on the os basale (Fig. 1A). The lateral side of the element also overlays the dorsal facet of the lateral wall of the os basale. The lateral edge of the element bears a facet for the squamosal and a foramen that leads to a canal that bifurcates and opens dorsally (Fig. 3E). Norris and Hughes (1918) reported this to be for the passage of a sensory branch of the trigeminal nerve arising from the dorsal side of the Gasserian ganglion, which in amphibians is generally referred to as the ‘dorsal fifth’. Ventrally, the parietal has an elongate depression at its anteriormost end, close to the median fissure, which accommodates the dorsomedial process of the sphenethmoid.

Squamosal

The squamosal forms most of the lateral surface of the ‘cheek’ region, and it lies ventrolateral to the frontal and parietal, and posterior to the maxillopalatine (Fig. 1A, B).

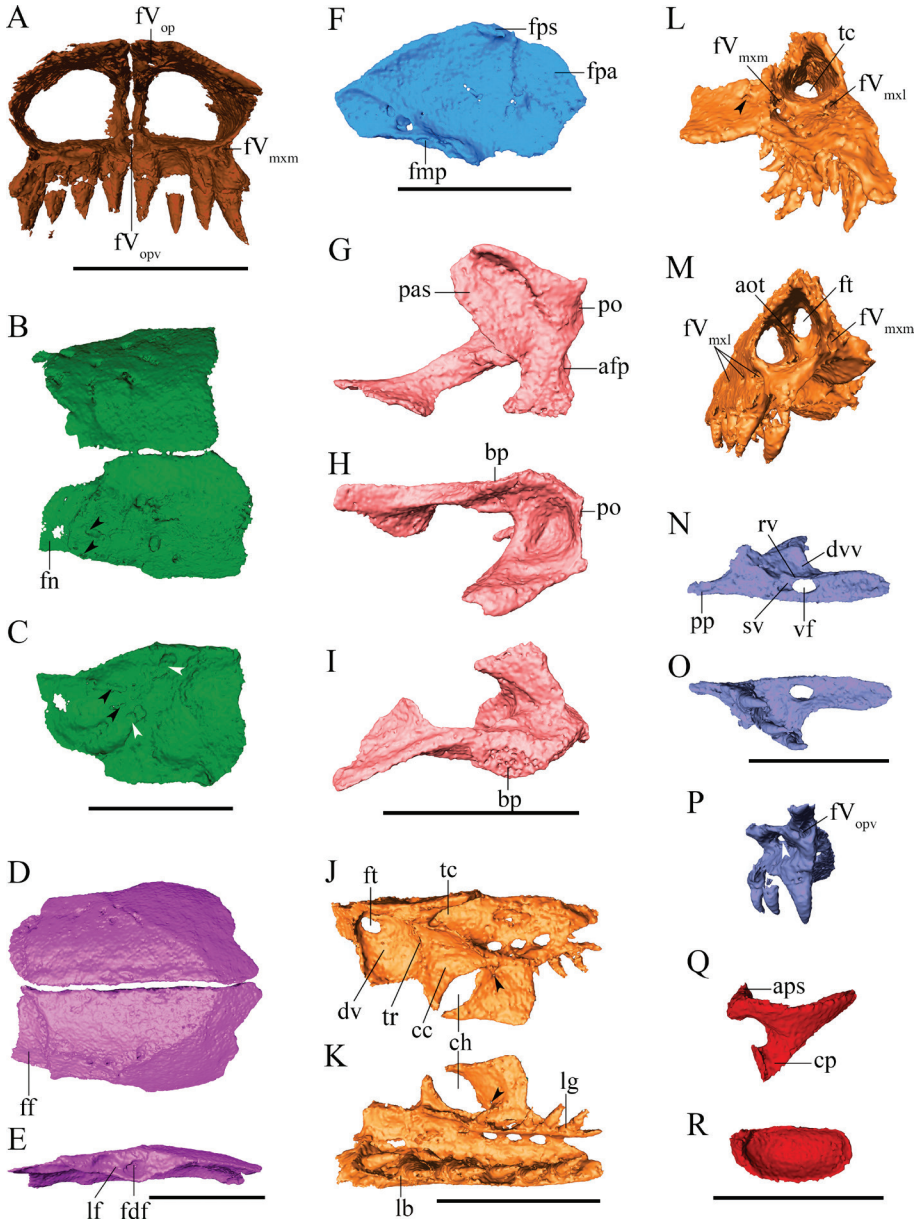

Figure 3. The dermatocranial elements and stapes of *Gegeneophis carnosus* (RAM 0020). **A** posterior view of the nasopremaxillae; **B** dorsal view of the frontals (arrowheads indicate foramina for branchlets of the ophthalmic division of the trigeminal nerve): **C** ventral view of the left frontal (black arrowheads indicate foramina for branchlets of the ophthalmic division of the trigeminal nerve; white arrowheads indicate the channel for a branch of the ophthalmic division of the trigeminal nerve); **D** dorsal view of the parietals; **E** lateral view of the left parietal; **F** medial view of the right squamosal; **G**–**I** left pterygoquadrate in **G** lateral view; **H** medial view; **I** ventral view; **J**–**M** the right maxillopalatine in **J** dorsal view (arrowhead indicates the internal apical foramen on the maxillopalatine posterior to the choana); **K** ventral view (arrowhead indicates the internal apical foramen on the maxillopalatine posterior to the choana); **L** posterior view (arrowhead indicates the internal apical foramen on the maxillopalatine posterior to the choana); **M** anterior view; **N**–**P** the right vomer in **N** dorsal view; **O** ventral view; **P** anterior view (arrowhead indicates the foramen serving as an anterolateral opening of the sulcus on vomer); **Q**–**R** the left stapes in **Q** dorsal view; **R** internal view showing the footplate. Scale bars: 1 mm.

Anteriorly it lies between frontal and maxillopalatine (Fig. 1B). A short facet for the parietal is present near the inner posterior border, opposite to the aforementioned lateral foramen on the parietal (Figs 1A, 3F). The outer anterior border of the squamosal has a lateral facet for the maxillopalatine (Figs 1B, 3F). Four foramina, one larger than the others, are present immediately dorsal to this facet. A shallow channel on the internal surface of the squamosal connects to these foramina (Fig. 3F). The posterior internal surface of the squamosal has a facet (Fig. 3F) for the processus ascendens (*sensu* Ramaswami 1942) of the pterygoquadrate. Immediately anterior to this lie a few foramina (Fig. 3F) presumed to be part of a common canal for nerves and/or blood vessels. According to Norris and Hughes (1918), the lateral branch of the maxillary division of the trigeminal nerve and lateral sensory branch of the mandibular division of the trigeminal nerve pass through the squamosal of caecilians. A lateral facet for articulation with the pterygoquadrate is present on the outer posteriormost region of the squamosal (black arrowhead in Fig. 1B).

Pterygoquadrate

The pterygoquadrate comprises a short but broad quadrate portion and a long spatulate pterygoid portion (Fig. 3G–I). The processus ascendens is broad, forming an expanded articulation with the squamosal (Figs 1B, 3G). The barely developed processus oticus articulates with the columellar process of the stapes (Figs 1B, 3G), and the adjoining articular facet articulates with the pseudoangular of the lower jaw (Fig. 3G). The processus oticus is a small, slightly depressed surface, and the articular facet for the pseudoangular is concave (Fig. 3G). The inner surface of the base of the pterygoquadrate anterior to the processus oticus is deeply depressed (Fig. 3H). The basal process of the element lies close to this depression, articulating with the basicranial articulation of the os basale (Figs 1C, 3H, I). The spatulate pterygoid part of the element displays some torsion about its long axis, and the ventral surface articulates with the posterior terminus of the palatine shelf (Figs 1C, 3I). The anterior terminus of the pterygoid part extends close to the palatine shelf posterior to the choana (Fig. 1C).

Maxillopalatine

The maxillopalatine is dentigerous, irregularly shaped with a maxilla part laterally and palatine part ventrally with an extension that forms most of the choanal border (Fig. 1B, C). The palatine part posterior to the choanae is broader than that to the anterior, and it encloses a small internal apical foramen (arrowheads in Fig. 3J–L). The right and left bones have six and seven labial teeth, along with two and one replacement teeth, respectively, and four and five lingual teeth on the left and right maxillopalatines, respectively, with a single replacement tooth on each. There is a socketless gap, the size of the base of a single tooth, between the last vomerine and first maxillopalatine teeth. The labial teeth are larger than the lingual teeth (Fig. 3K).

More than a dozen foramina are found throughout the bone. Oval foramina, two on the left maxillopalatine (not shown in the figure) and three on the right (Fig. 3J, K), lie posterior to the beginning of the tentacular canal, perforating the palatine shelf. Two other foramina (Fig. 3L, fV_{mxl}, fV_{mxm}) are associated with small channels running ventrolateral to the tentacular canal, likely carrying the two branches of the maxillary division of the trigeminal nerve. One of these channels (Fig. 3L, fV_{mxl}), presumed to be for the passage of the lateral branch of the maxillary division of the trigeminal nerve, connects to a few lateral foramina (Fig. 3M, fV_{mxl}). The other channel (Fig. 3L, fV_{mxm}), presumed for the passage of the medial branch of the maxillary division of the trigeminal nerve, connects to a few foramina on the internal and ventral surface and to a terminal foramen at the anterior of the element, immediately posterolateral to the anterior opening of the tentacular canal (Fig. 3M, fV_{mxm}). This channel for the medial branch of the maxillary division of the trigeminal nerve continues its course through the previously described lateral bony channel on the nasopremaxilla (Figs 1B, 3A).

Additionally, the dorsal surface of the maxilla enclosing the tentacular canal bears three or four foramina. A foramen at the anterolateral side of the maxillopalatine, dorsal to the anterior opening of the tentacular canal (Fig. 1B), is presumed to transmit a branch of the ophthalmic division of the trigeminal nerve.

A large foramen (Fig. 3J, M, ft) lying lateral to the anterior of the tentacular canal, opens into it from a large anterodorsal depression on the maxillopalatine (Fig. 3J, dv). We do not yet have direct information on cranial soft-tissue structures in *G. carnosus* but, based on other caecilians (e.g., Ramaswami 1941; Sarasin and Sarasin 1887–1890; Billo and Wake 1987; Schmidt and Wake 1990, Himstedt and Simon 1995), the depression on the floor of the anterior of the dorsal surface of the maxillopalatine is interpreted as holding, at least in part, the vomeronasal organ (Fig. 3J). The large foramen that communicates between the anterolateral corner of this depression for the vomeronasal organ and the lateral surface of the anterior of the tentacular canal likely transmits at least the tentacular (nasolacrimal) duct (Fig. 3J, M). The posterior end of the depression for the vomeronasal organ is bordered by a transverse ridge that divides it from an additional concavity that is bordered by this ridge, by the medial wall of the tentacular canal, and by the choana (Fig. 3J). This cavity likely holds the Choanenschleimbeutal (e.g., Sarasin & Sarasin 1887–1890; 'choanal mucous sac').

Vomer

The vomer is longer than wide, having three functional teeth on its lingual row, along with a single replacement tooth on each bone (Fig. 1C), and is widest at the posteriormost tooth socket (Fig. 3N, O). The premaxillary process of the vomer is elongate, narrow, and not visible from the ventral view of the skull because it is inserted into the nasopremaxillae. The oval vomerine foramen is located at the centre of the bone (Figs 1C, 3N, O).

The depression on the dorsal surface at the anterior end of the maxillopalatine for the vomeronasal organ extends onto the lateral part of the dorsal surface of the vomer (Fig. 3N). Here, the concavity's medial edge is delimited by a ridge on the vomer that curves anteriorly and laterally from the vomerine foramen to meet the ridge on the maxillopalatine that forms the anterior border of the depression for the vomeronasal organ (Figs 3J, N). There is no development of an olfactory eminence on the floor of the olfactory chamber, on either the anterior of the vomer or the posterior of the nasopremaxilla. Thus, there is no partial longitudinal subdivision into medial and lateral olfactory chambers.

The dorsal surface of the vomer bears a short sulcus (Fig. 3N) that extends from the anterior margin of the vomerine foramen to a closed channel that opens anterolaterally on the vomer as a foramen above the dental margin (arrowhead in Fig. 3P). A lateral flange is present dorsal to this anterolateral foramen, abutting both the pos-

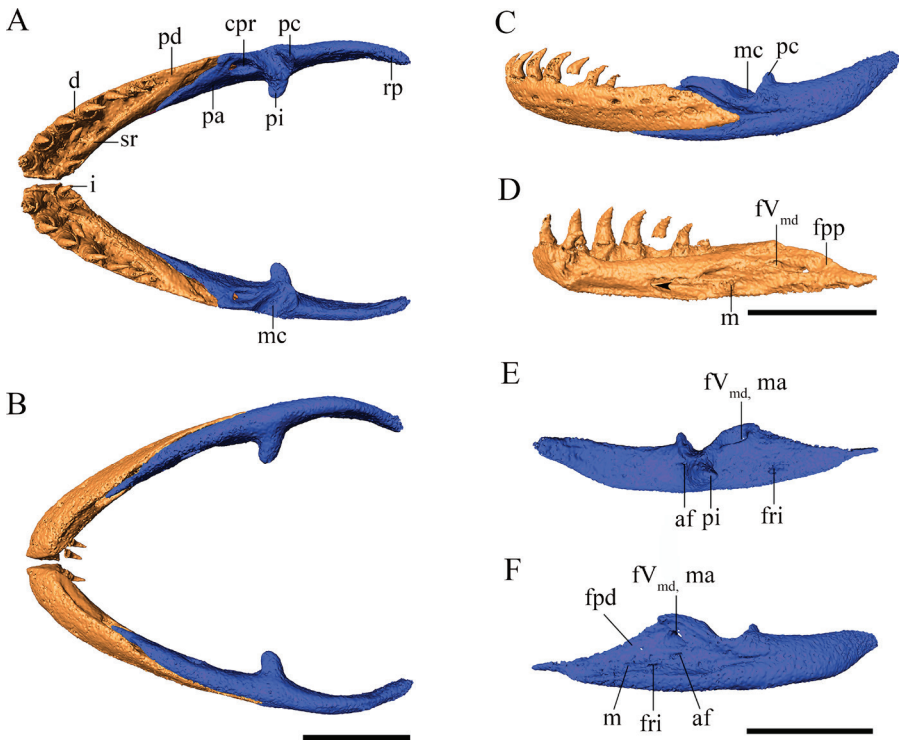

Figure 4. The lower jaw of *Gegeneophis carnosus* (RAM 0020). **A** dorsal view; **B** ventral view; **C** lateral view; **D** medial view of pseudodentary; **E**–**F** the pseudoangular in **E** medial view; **F** lateral view. Scale bars: 1 mm.

terior of the premaxillary portion of the nasopremaxilla and the inner anterior terminus of the palatine shelf (Figs 1C, 3P). An additional anterior foramen is present, immediately ventral to the base of the premaxillary process of the vomer (Fig. 3P, fV_{opv}), anterior to the aforementioned anterolateral foramen, likely carrying the ventral branch of the ophthalmic division of the trigeminal nerve. This nerve branch presumably also passes through the medial foramen on the floor of the nasopremaxilla, as mentioned earlier (Fig. 3A).

Stapes

The imperforate stapes forms a lateral joint between the os basale and pterygoquadrate (Fig. 1B, C). It has an elongate, concave, and nearly elliptical footplate and a short, laterally projecting columellar process, which articulates the processus oticus of the pterygoquadrate (Figs 1B, C, 3Q, R). The footplate closely fits within the fenestra ovalis (Fig. 1B, C). The footplate bears a small process at its apex, inserted into the void between the foramina for the ventral vein and the facial nerve in the antotic wall of the os basale (Figs 2D, 3Q, R).

Lower Jaw

The tip of the lower jaw is subterminal, being overhung by the anterior of the snout by approximately 0.75 mm when in articulation with the skull. It is composed of extensively overlapping units of dentigerous pseudodentary and edentulous pseudoangular. They form a non-kinetic articulation that makes them a single mechanical unit (Fig. 4A–C). The pseudodentary is broadest at its anterior terminus and narrowest at its posterior terminus (Fig. 4A, D). The pseudodentary has a ‘splenial’ ridge bearing inner (lingual) mandibular teeth at its anterior terminus (Fig. 4A, B). A trough-like fossa bearing two (on the right) or three (left) foramina are present between the ‘splenial’ ridge and outer tooth row (Fig. 4A).

The posterior of the medial surface of the pseudodentary bears a large, anteriorly tapering region (Fig. 4D) that laterally overlaps (and articulates with) the pseudoangular. A small knob near the centre of this region of the pseudodentary is interpreted as a meckelian bone (Fig. 4D), the ossified remnant of Meckel’s cartilage of earlier ontogenetic stages (e.g., see Müller 2006). The region also bears two foramina; one anterior and the other posterodorsal to the meckelian bone (Fig. 4D). The anterior foramen (arrowhead in Fig. 4D) leads to an internal channel that connects to the foramina on the fossa between the ‘splenial’ ridge and outer tooth row and to another foramen lingual to the ‘splenial’ ridge. The more posterodorsal foramen (Fig. 4D, fV_{md}) leads to another internal channel that connects to more than a dozen foramina (17 on the left pseudodentary and 14 on the right) on the lateral surface of the pseudodentary (Fig. 4C). The latter foramina and channel transmit the branchlets of the mandibular division of the trigeminal nerve, which enters the lower jaw via the canalis primordialis (Fig. 4A). Seven large outer (labial) and two smaller inner mandibular teeth occur on the lower jaw. Additionally, two replacement teeth are present on either side, close and immediately lingual to the third and sixth outer row teeth (Fig. 4A), and one replacement tooth lingual to the inner mandibular teeth on either side.

The pseudoangular is an elongate bone with a pointed anterior terminus inserted into the pseudodentary, and a prominent, slightly curved, and upwardly directed retroarticular process at its posterior end (Fig. 4A–C, E, F). The facet on the pseudoangular for the posterior terminus of the laterally overlapping pseudodentary is triangular, tapering both anteriorly and posteriorly (Fig. 4F). A small meckelian bone lies near the centre of the region overlapped by pseudodentary (Fig. 4F). The medial surface of the pseudoangular bears the medially directed processus internus (Fig. 4A, B, E). The processus condyloideus, posterodorsal to the processus internus, forms the posterior border of the deep, somewhat U-shaped (in section) mandibular cotyle—the surface for articulation with the pterygoquadrate of the skull (Fig. 4A, C, E, F).

The canalis primordialis, through which the mandibular division of the trigeminal nerve and the mandibular artery pass, lies immediately anterior to the mandibular cotyle and opens as an oval foramen on the region overlapped by the pseudodentary (Fig. 4A, E, F). The foramen transmitting the ramus intermandibularis of the trigeminal nerve lies anteroventral to the foramen for the mandibular division of the trigeminal nerve and the mandibular artery (Fig. 4E, F). The alveolar foramen for transmission of the alveolar branch of the facial nerve lies immediately posterior to the junction of processus condyloideus and processus internus, and is continuous with a narrow channel opening to the region overlapped by the pseudodentary (Fig. 4E, F).

Vertebral column

Total number of vertebrae, from nine specimens, ranges from 123 to 130, with a mean of 126.7 (standard deviation ±2.4). The µCT-scanned specimen has 129 vertebrae. The vertebral centra are amphicoelous except for those of the atlas and terminal vertebra. Except for the atlas and terminal vertebra, other vertebrae have associated bicipital ribs. Tail vertebrae are absent because the species has a near-terminal vent and lacks a true tail. A sacral region is also absent. Neural arch and centrum are common for all vertebrae. All vertebrae lack a haemal arch.

Atlas

The atlas is characterised by the presence of a large, bipartite atlantal cotyle (Fig. 5A4) that articulates with the occipital condyle of the skull. The atlantal cotyle is shallowly concave, and the spinal root foramen lies ventral to it (Fig. 5A5). The atlas lacks ribs and associated processes. The neural arch is shorter than the succeeding vertebrae, and the centrum is very short (Fig. 5A1–3). The anterior of the centrum is very narrow, with a blunt end (Fig. 5A4), and the oval-shaped posterior surface has a broad concavity with a deeper central cavity (Fig. 5A5). The postzygapophysis of the atlas articulates with the prezygapophysis of the axis. A prezygapophysis, longitudinal nuchal ridge, parasphene (basapophysis), ventral keel (hypapophyseal keel), and hypapophysis are absent.

Axis and axial ribs

The axis, the second vertebra, articulates with the atlas anteriorly via its prezygapophyses and the anterior face of the centrum, and it articulates with the third vertebra posteriorly via the postzygapophyses and the posterior face of the centrum. The axis is the anteriormost rib-bearer of the column. The ribs, which are stout, mostly straight, and with blunt termini, terminate posteriorly before the level of the postzygapophyses (Fig. 5B1). The rib is bicipital, its capitulum articulates with the parapophyseal facet ventrally, and its tuberculum articulates with the diapophyseal facet dorsally (Fig. 5B1–3). The parapophysis is prominent, and it presents a flat articular facet anteroventrally (Fig. 5B2). A pair of spinal nerve foramina are present between the para- and diapophyses (Fig. 5B3). The neural arch is prominent (Fig. 5B1). The centrum is hourglass-shaped with deep concavities on the anterior and posterior articular faces (Fig. 5B2, 4, 5). A longitudinal nuchal ridge is present (Fig. 5B1, 3), and the ventral keel is very prominent (Fig. 5B2) with a hypapophysis. The midline of the neural arch has a prominent rounded anterior projection (Fig. 5B1). Anteroventrally, parasphene is absent.

Third and fourth vertebrae and ribs

The third and fourth vertebrae are similar to the axis in having a longitudinal nuchal ridge, pre-and postzygapophyses, parapo- and diapophyses, ribs, and ventral keel. In addition, they also possess a pair of anteroventral parasphenes for articulation with the preceding vertebra. The ribs are straight and slightly longer than the ribs of the axis. The rib capitulum is considerably longer than the tuberculum. The para- and diapophyses are less prominent than on the axis. A pair of spinal nerve foramina are present between the para- and diapophyses. The midline of the neural arch anterior to the longitudinal nuchal ridge on the third vertebra has a more rounded projection than that of the axis, and it is pointed in the fourth vertebra. The nuchal ridge is slightly more prominent than that on the axis.

Midbody vertebrae

The neural arch and hourglass-shaped centrum of the midbody vertebrae are longer than those in the third and fourth vertebrae (Fig. 5C1, 2). The parasphenes are prominent (Fig. 5C2). The facets for articulation with the rib tuberculum and capitulum are not on raised (di- or par-) apophyses. The ribs are curved in dorsal and ventral views, and are laterally compressed with a pointed terminus (Fig. 5C1, 2). The rib capitulum is substantially longer than the tuberculum (Fig. 5C3). A longitudinal nu-

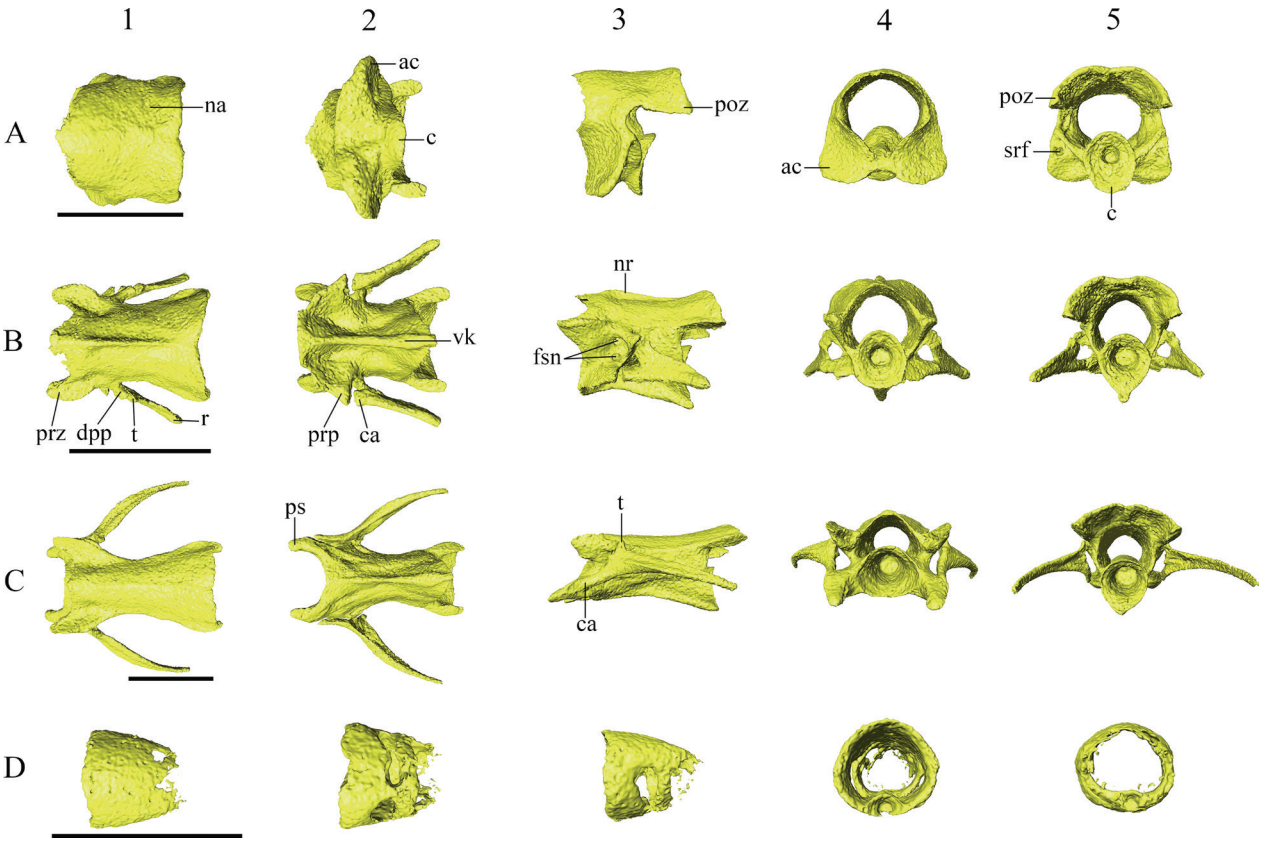

Figure 5. The vertebrae of *Gegeneophis carnosus* (RAM 0020). Rows: **A** atlas; **B** axis; **C** mid-body vertebra; **D** last vertebra. Columns: **1** dorsal view; **2** ventral view; **3** lateral view; **4** anterior view; **5** posterior view. Scale bars: 1 mm

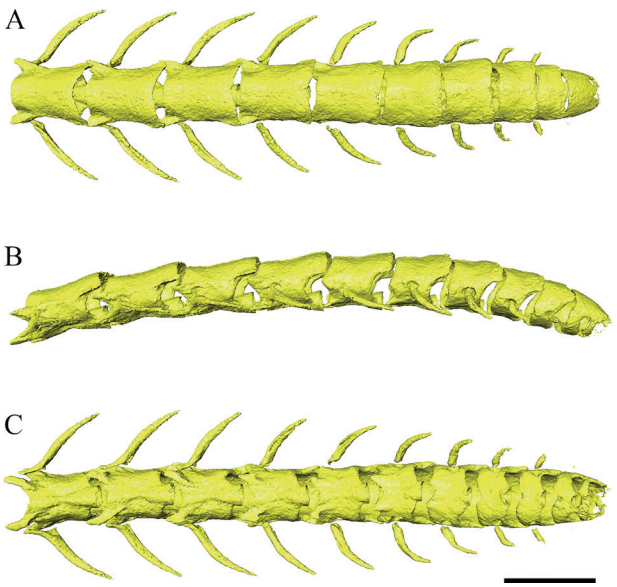

Figure 6. The posteriormost ten vertebrae of *Gegeneophis carnosus* (RAM 0020). **A** dorsal; **B** lateral; **C** ventral views. Scale bar: 1 mm.

chal ridge is absent dorsally. A ventral keel and a hypapophysis are present (Fig. 5C2). Each vertebra articulates with the preceding vertebra via the prezygapophyses, parasphenes, and the anterior of the centrum, and with the succeeding vertebra via the postzygapophyses and posterior of the centrum. The concavities on the anterior and posterior articular surfaces of the centrum are deeper in the midbody vertebrae than in the anteriormost vertebrae (Fig. 5C4, 5). Most vertebral dimensions and rib length are at a maximum in the midbody vertebrae and smaller towards the anterior and posterior ends of the column.

Posteriormost ten vertebrae

As noted in the previous section, the vertebral dimensions reduce considerably in the posteriormost vertebrae. The length of the neural arch and centrum reduces substantially in the posteriormost five vertebrae (Fig. 6A–C). The neural arch and centrum of the terminal vertebra are longer than those of the preceding vertebra (Figs 5D, 6A–C). The centra maintain an hourglass shape throughout the vertebral column, though they are less strongly waisted posteriorly (Fig. 6C). The ribs are very short (rudimentary) in the posteriormost second and third vertebrae (Fig. 6A–C). The last vertebra lacks ribs (Fig. 5D). However, tiny bony remnants on either side can be seen in the positions where ribs would be expected. The tuberculum and capitulum and diapo- and parapophyses are not distinguishable after the seventh posteriormost vertebra (Fig. 6A–C). The parasphene is substantially reduced after the ninth posteriormost vertebra and absent in the posteriormost four vertebrae (Fig. 6C). The prezygapophyseal process is poorly developed in the fifth posteriormost vertebra and absent thereafter (Fig. 6A). A longitudinal nuchal ridge is absent, and the ventral keel is poorly demarcated and completely absent in the last four vertebrae (Fig. 6A–C).

Discussion

Comparative osteology of *Gegeneophis*

This is the first detailed study of the osteology of *Gegeneophis carnosus* since it was described by Beddome (1870) from two specimens from northern Kerala. Descriptive studies of the skeletal system of *Gegeneophis* have thus far been limited to works on *G. ramaswamii* (e.g., Ramaswami 1942, 1947; Taylor 1969, 1977a, 1977b; Müller et al. 2005; Maddin 2011; Maddin et al. 2012). Sherratt et al. (2014) and Bardua et al. (2019) included *G. ramaswamii* and *G. carnosus* in their broad, quantitative analyses of caecilian cranial shape. Thus, our study improves understanding of interspecific skeletal variation within *Gegeneophis* and within caecilians more generally.

The cranium of *G. carnosus* differs from that of *G. ramaswamii* in some details (Figs 1A–C, 2A–C; Ramaswami 1942: plate 12; Maddin et al. 2012: fig. 6). The choanal area in contact with vomer is smaller in *G. carnosus*. The parietal expansion towards the os basale is slightly less in *G. ramaswamii* (pers. obs.; Ramaswami 1942: plate 12). A process in the anterior of the footplate was not reported for the stapes of *G. ramaswamii* (Maddin et al. 2012). The sphenethmoid is covered by the dermatocranial elements in *G. carnosus*, being only slightly visible in the dorsal view through the median fissure. Such visibility is not discernible in Ramaswami's (1942) drawing of *G. ramaswamii* (incorrectly reported as *G. carnosus* in his study), but our personal observation of the skull of cleared and stained material of *G. ramaswamii* (unpublished data) showed a similar condition to that we document in *G. carnosus*.

As in *G. ramaswamii*, the sphenethmoid of *G. carnosus* lacks sola nasi and ventral flanges. The dorsal facet of the nasal septum of *G. ramaswamii* is broader than that of *G. carnosus*. The height of the nasal septum declines sharply anteriorly in *G. carnosus* but gradually in *G. ramaswamii*. The sphenethmoid of *G. carnosus* has an anterolateral expansion from its lateral wall in contrast to the anterolateral process of *G. ramaswamii*. The anterolateral expansion in *G. carnosus* is more anteriorly projecting than the anterolaterally projecting anterolateral process of *G. ramaswamii*. The posterior of the dorsomedial process of the sphenethmoid of *G. carnosus* is narrower than in *G. ramaswamii*, and it gradually forms an acute terminus, unlike the abrupt acute posterior end of the dorsomedial process of the latter (Maddin et al. 2012).

Interspecific variation is also observed in the position of the foramina for the dorsal and ventral trunk of olfactory nerves in the sphenethmoid; both foramina are closer to the midline in *G. carnosus*. The number of foramina for medial branch of the vestibulocochlear nerve also varies in both species: one in *G. carnosus* and two in *G. ramaswamii*. The incision of the lateral wall of the sphenethmoid and antotic wall of the os basale by the optic foramen is deep and equal in *G. carnosus* versus unequal in *G. ramaswamii*. The facet for the pterygoquadrate in the antotic wall is less pronounced in *G. carnosus* than in *G. ramaswamii*. The parasphenoid rostrum reaches only to the base of the nasal septum in *G. carnosus* but to the midpoint of the septum in *G. ramaswamii*. The ventral wing-like projection of the otic capsule in *G. carnosus* is not as prominent as in *G. ramaswamii*. The insertion of the apical process of the footplate of stapes into the void in the antotic wall observed in *G. carnosus* has not been reported for *G. ramaswamii*. A similar void is not discernible in the os basale of *G. ramaswamii* (Maddin et al. 2012).

Comparative osteology of grandisoniids

Gegeneophis carnosus is one of 12 currently recognised species of *Gegeneophis* (Kotharambath et al. 2015), all endemic to peninsular India. *Gegeneophis*' closest relative is *Indotyphlus*, the two species of which are also endemic to this region (Giri et al. 2004). These two genera are the only Asian representatives of the family Grandisoniidae (= Indotyphlidae of e.g., Wilkinson et al. 2011), the others comprising *Praslinia*, *Hypogeophis* and *Grandisonia* (Seychelles; 8 species), *Sylvacaecilia* (Ethiopia; 1 species) and *Idiocranium* (Cameroon; 1 species) (Frost 2021). Descriptions of caecilian skeletal morphology are generally sparse, and that is true also for grandisoniids. However, the osteology of *Hypogeophis rostratus* has received some attention over the last 150 years (e.g., Wiedersheim 1879, Peter 1894, Wake 2003), and a few studies have examined the osteology of *Grandisonia* species (e.g., Straub 1985) and *Idiocranium russeli* (a small, possibly miniaturized taxon) (Wake 1986; Theska et al. 2018; Marshall et al. 2019). Wake (1987) examined the osteology of *Sylvacaecilia grandisonae*, and Taylor (1970) briefly described the skull of *Indotyphlus battersbyi.*

The absence of an orbit is the major difference between *Gegeneophis* and all other confamilial taxa (Wake 2003; Wilkinson et al. 2011). This lack is associated with a proportionately larger maxillary portion of the maxillopalatine in *G. carnosus*. The sphenethmoid is not exposed dorsally in *G. carnosus* and *G. ramaswamii* but is in *H. rostratus* (slightly) and *I. russeli* (Wilkinson et al. 2011; Theska et al. 2018; Marshall et al. 2019). The expansion of the parietal towards the os basale in *G. carnosus* and (lesser in) *G. ramaswamii* is also observed in *Idiocranium russeli* but not in other grandisoniids (Parker 1941; Wake 1987; Wilkinson et al. 2011; Theska et al. 2018; Marshall et al. 2019).

In *G. carnosus* and *G. ramaswamii*, the tentacular aperture lies at the extremity of maxillopalatine, but in *Sylvacaecilia grandisonae* and *Grandisonia alternans*, it is midway between the eye and nostril; in *Indotyphlus* it is closer to the eye than the nostril, and in *Praslinia cooperi* it is adjacent to the eye (Taylor 1970; Carroll and Currie 1975; Wake 1987; Wilkinson et al. 2011). The tentacular canal of *G. carnosus* and *G. ramaswamii* is closed (roofed laterally) but is partly open in *S. grandisonae* and fully open in *Indotyphlus* (Wake 1987; Wilkinson et al.

2011). The covering of the parasphenoid rostrum by the vomer is less substantial in other grandisoniids than in *G. carnosus* and *G. ramaswamii*. *Grandisonia* spp. have a bony olfactory eminence partially dividing the olfactory chambers longitudinally into medial and lateral cavities (Wilkinson et al. 2011); this structure is absent in *G. carnosus* and *G. ramaswamii.*

The braincase of *G. carnosus* also differs notably from that of other (non-*Gegeneophis*) grandisoniids. The sola nasi is present in *Grandisonia alternans* (Maddin et al. 2012: fig. S12), though the text of that publication reports the absence of sola nasi for the family. The anterolateral expansion is absent in *Idiocranium russeli*; in *G. alternans* and *H. rostratus*, an anterolateral process is present which is narrower and slightly more elongated than the anterolateral expansion of *G. carnosus*. The dorsal facets of both the lateral wall of the sphenethmoid and the antotic wall of the os basale are wider in *H. rostratus* than in *G. carnosus* and *G. ramaswamii*. The foramina for the ventral branches of the olfactory nerve are more widely separated in *G. alternans* and *H. rostratus* than in *G. carnosus* and *G. ramaswamii*, and the former two species lack separate foramina for the dorsal and ventral veins. However, in *I. russeli*, there is a separate foramen for the ophthalmic division of the trigeminal nerve in the antotic wall. When compared with the void observed in the antotic wall of *G. carnosus*, the foramen that Maddin et al. (2012) identified as for the ventral vein in *I. russeli* (Maddin et al. 2012: fig. S14) looks unlikely because the foramen posterior to it probably is the one for the ventral vein.

It is not fully clear whether the differences summarized above can be explained by phylogenetic signal, intraspecific variation and/or function. Features such as the closed orbit shared by *G. carnosus* and *G. ramaswamii* are putatively synapomorphic. However, more comparative data are needed for more specimens and for more congeneric species, and greater sampling and resolution for grandisoniid phylogeny (e.g., Gower et al. 2011, 2016) will be required to more fully test and clarify this.

Intraspecific variation and asymmetry

We documented asymmetry in the structure and size of the left and right frontals and parietals of *G. carnosus*; a structural variation on the facet overlain by the preceding bone. Minor variations were also observed in the position, size, and occasionally the number of foramina on the left and right sides of the skull. The number of dorsal foramina on the nasopremaxilla is four on the left and five on the right. Though the number is the same, the size and distribution of foramina on the left and right frontals are also different. Squamosals and maxillopalatines also show variations in the number, distribution, and size of the foramina. The size of the foramina on one side is comparatively larger than that on the other side if the number of foramina is less on that side.

We observed replacement teeth on all dentigerous bones of *G. carnosus*. Tooth counts slightly differ for all series except for inner mandibular from the type specimens described by Taylor (1968): premaxillary-maxillary (this study) 21 (11 left, 10 right) vs 25 (Taylor 1968); vomeropalatine 15 (7 left, 8 right) vs 24; dentary 14 vs 19–20; inner mandibular 4 (left 2, right 2) vs 4. CT scan data for other specimens (including the types) of *G. carnosus* (Sherratt et al. 2014; Bardua et al. 2019) were not available to us for this study, but comparison with them will present further opportunity to assess osteological intraspecific variation in this taxon.

Detailed accounts of vertebral anatomy are not available for other grandisoniids, so intrafamilial variation cannot yet be assessed. The vertebral column of *G. carnosus* has a similar general pattern to that described for other tailless caecilians (e.g., see Wake 1980 for *Dermophis mexicanus*). Although the last few vertebrae generally become shorter, the last vertebra is longer than the penultimate one. There is a clear but incomplete (restricted to the lower surface) transverse gap near the middle of the last vertebra, suggesting this vertebra might be a fusion of two vertebrae, at least of their neural arches. Wake (1980) noted the fusion of posterior vertebrae in sets of two or three in *D. mexicanus*. As reported by Lowie et al. (2022) for other caecilians, the vertebral column of *G. carnosus* is heterogenous without being regionalized.

Functional considerations

The cranium of *G. carnosus* resembles that of *G. ramaswamii* in bearing features that have been interpreted as adaptations to head-first burrowing in presumably highly fossorial caecilians, such as a subterminal mouth, closed (absent) orbit, and a compact, stegokrotaphic skull (e.g., Taylor 1968; Wake and Hanken 1982; Nussbaum 1983; Wake 1993; Nussbaum and Pfrender 1998; O'Reilly et al. 2000; Kleinteich et al. 2012; Sherratt et al. 2014). However, quantitative baseline field ecological data for caecilians, in general, are sparse (e.g., Gower et al. 2004b; Kupfer et al. 2005; Bardua et al. 2019), and compelling functional evidence to support the generality of the adaptive value of these cranial features to dedicated fossoriality in caecilians is lacking (Ducey et al. 1993; Herrel and Measey 2010; Kleinteich et al. 2012; Lowie et al. 2021).

As far as we know, all reported *G. carnosus* specimens have been dug from soil or found under cover objects and not found in loose leaf litter or moving on the surface, in contrast to broadly sympatric ichthyophiids that are occasionally observed in these microhabitats (pers. obs.). Thus, we believe that individuals of *G. carnosus* are largely fossorial and spend most of their lives in soil, and we consider this species' cranial morphological features as likely explained to a substantial degree by adaptations to their fossoriality. However, we lack quantitative field ecological data to test this, or functional data or behavioural observations that might allow other explanations of stegokrotaphy and closed orbits to be tested (such as variation in angle of the head during burrowing: Kleinteich et al. 2012, or protection of soft tissues from potentially harmful prey: Wilkinson et al. 2013).

Closing remarks

The phylogenetic relationships of species of *Gegeneophis* are incompletely resolved (Gower et al. 2011, 2016). The closest known relative of *G. carnosus* is inferred to be *G. primus* (Gower et al. 2016), but the closest relative(s) of this sister pair remain(s) unknown. Thus far, phylogenetic relationships of *Gegeneophis* spp. have been inferred using DNA sequence data (Gower et al. 2011, 2016). In addition to expanding the available molecular genetic data (especially for nuclear genes), advancing understanding of *Gegeneophis* spp. phylogeny will likely be aided by further comparative studies of morphology, including of the skeletal system. Species of *Gegeneophis* are ecophenotypically diverse in features such as annulation, scalation, body proportions, visibility of the eye, dentition, and reproductive mode (e.g., Giri et al. 2003; Bhatta et al. 2007; Gower et al. 2008; Kotharambath et al. 2012, 2015), and these aspects of the phenotype might yield useful phylogenetic data. We view the present description of the osteology of *G. carnosus* as a step towards being able to integrate skeletal morphology in a fuller understanding of *Gegeneophis* ecophenotypic variation, its evolutionary patterns, and its functional causes.

Conflict of Interest

The authors have declared that no competing interests exist.

Acknowledgements

SRP is grateful to CSIR, Government of India, New Delhi for a PhD fellowship. RK was supported by a Start-Up Grant from the University Grants Commission, Government of India, New Delhi, and a DBT-Stanford Foldscope Grant from the Department of Biotechnology, Government of India, New Delhi. RK and DJG were also supported by a Visiting Advanced Joint Research (VAJRA) award from the Science and Engineering Research Board of the Department of Science and Technology, Government of India. The Dept. of Forests, Government of Kerala is thanked for a research permit. Dr Sheetal Kalme and Sunil Prabhakar at C-CAMP in NCBS-TIFR Campus provided help during the µCT scanning. SRP and RK are grateful to Ranjith Vengot for his help at NCBS and Krishna Medical Centre and Sulu Mohan for her help at NCBS. The authors thank Krishna Medical Centre, Kanhangad for permitting the use of their X-ray facility, and Nikhil Ramachandran for his technical assistance. The submitted manuscript was improved by review comments from Alex Kupfer. Hendrik Müller provided helpful discussion about some anatomical details.

References

Bardua C, Wilkinson M, Gower DJ, Sherratt E, Goswami A (2019) Morphological evolution and modularity of the caecilian skull. BMC Evolutionary Biology 19(30): 1–24. https://doi.org/10.1186/s12862-018-1342-7

Beddome RH (1870) Descriptions of new reptiles from the Madras Presidency. Madras Monthly Journal of Medical Science 2: 169–176.

Bhatta G, Dinesh KP, Prashanth P, Kulkarni NU (2007) A new species of the Indian caecilian genus *Gegeneophis* Peters (Amphibia: Gymnophiona: Caeciliidae) from the surroundings of Mahadayi Wildlife Sanctuary, Western Ghats. Current Science 93(10): 1442–1445.

Billo R, Wake MH (1987) Tentacle development in *Dermophis mexicanus* (Amphibia, Gymnophiona) with an hypothesis of tentacle origin. Journal of Morphology 192(2): 101–111.

Carroll RL (2007) The Palaeozoic ancestry of salamanders, frogs and caecilians. Zoological Journal of the Linnean Society 150(1): 1–140. https://doi.org/10.1111/j.1096-3642.2007.00246.x

Carroll RL, Currie PJ (1975) Microsaurs as possible apodan ancestors. Zoological Journal of the Linnean Society 57: 229–247.

Dubois A, Ohler A, Pyron RA (2021) New concepts and methods for phylogenetic taxonomy and nomenclature in zoology, exemplified by a new ranked cladonomy of recent amphibians (Lissamphibia). Megataxa 5(1): 1–738.

Ducey PK, Formanowicz Jr DR, Boyet L, Mailloux J, Nussbaum RA (1993) Experimental examination of burrowing behavior in caecilians (Amphibia: Gymnophiona): effects of soil compaction on burrowing ability of four species. Herpetologica 49(4): 450–457.

Duellman WE, Trueb L (1986) Biology of Amphibians. McGraw-Hill, New York, 289–312 pp. https://doi.org/10.1002/mmnz.19890650217

Frost DR (2021) Amphibian Species of the World: an Online Reference. Version 6.1. (20.12.2021) Electronic database accessible at https://amphibiansoftheworld.amnh.org/index.php. American Museum of Natural History, New York, USA. https://doi.org/10.5531/db.vz.0001

Giri V, Gower DJ, Wilkinson M (2004) A new species of *Indotyphlus* Taylor (Amphibia: Gymnophiona: Caeciliidae) from the Western Ghats, India. Zootaxa 739: 1–19.

Giri V, Wilkinson M, Gower DJ (2003) A new species of *Gegeneophis* Peters (Amphibia: Gymnophiona: Caeciliidae) from southern Maharashtra, India, with a key to the species of the genus. Zootaxa 351: 1–10.

Gower DJ, Agarwal I, Karanth KP, Datta-roy A, Giri VB, Wilkinson M (2016) The role of wet-zone fragmentation in shaping biodiversity patterns in peninsular India: insights from the caecilian amphibian *Gegeneophis*. Journal of Biogeography 43: 1091–1102. https://doi.org/10.1111/jbi.12710

Gower DJ, Giri V, Dharne MS, Shouche YS (2008) Frequency of independent origins of viviparity among caecilians (Gymnophiona): Evidence from the first "live-bearing" Asian amphibian. Journal of Evolutionary Biology 21: 1220–1226. https://doi.org/10.1111/j.1420-9101.2008.01577.x

Gower DJ, Loader SP, Moncrieff CB, Wilkinson M (2004b) Niche separation and comparative abundance of *Boulengerula boulengeri* and *Scolecomorphus vittatus* (Amphibia: Gymnophiona) in an East Usambara forest, Tanzania. African Journal of Herpetology 53(2): 183–190. https://doi.org/10.1080/21564574.2004.9635510

Gower DJ, Mauro DS, Giri V, Bhatta G, Govindappa V, Kotharambath R, Oommen OV, Fatih FA, Mackenzie-Dodds JA, Nussbaum RA, Biju SD, Shouche YS, Wilkinson M (2011) Molecular systematics of caeciliid caecilians (Amphibia: Gymnophiona) of the Western Ghats, India. Molecular Phylogenetics and Evolution 59: 698–707. https://doi.org/10.1016/j.ympev.2011.03.002

Gower DJ, Wilkinson M, Oommen OV, Measey J, Dutta S, Bhatta G (2004a) *Gegeneophis ramaswamii*. The IUCN Red List of Threatened Species version 2021–3 (14.12.2021). Electronic database accessible at https://www.iucnredlist.org/species/59553/11962740.

Herrel A, Measey GJ (2010) The kinematics of locomotion in caecilians: effects of substrate and body shape. Journal of Experimental Zoology Part A: Ecological Genetics and Physiology 313(5): 301–309. https://doi.org/10.1002/jez.599

Himstedt W, Simon D (1995) Sensory basis of foraging behaviour in caecilians (Amphibia, Gymnophiona). Herpetological Journal 5(3): 266–271.

Kleinteich T, Maddin HC, Herzen J, Beckmann F, Summers AP (2012) Is solid always best? Cranial performance in solid and fenestrated caecilian skulls. Journal of Experimental Biology 215(5): 833–844. https://doi.org/ 10.1242/jeb.065979

Kotharambath R, Gower DJ, Oommen OV, Wilkinson M (2012) A third species of *Gegeneophis* Peters (Amphibia: Gymnophiona: Indotyphlidae) lacking secondary annular grooves. Zootaxa 3272: 26–34. https://doi.org/10.11646/zootaxa.3272.1.2

Kotharambath R, Wilkinson M, Oommen OV, Gower DJ (2015) A new species of Indian caecilian highlights challenges for species delimitation within *Gegeneophis* Peters, 1879 (Amphibia: Gymnophiona: Indotyphlidae). Zootaxa 3948(1): 60–70. https://doi.org/10.11646/zootaxa.3948.1.4

Kupfer A, Nabhitabhata J, Himstedt W (2005) Life history of amphibians in the seasonal tropics: habitat, community and population ecology of a caecilian (genus *Ichthyophis*). Journal of Zoology 266: 237–247. https://doi.org/10.1017/S0952836905006849

Lowie A, De Kegel B, Wilkinson M, Measey J, O'Reilly JC, Kley NJ, Gaucher P, Brecko J, Kleinteich T, Hoorebeke LV, Herrel A, Adriaens D (2021) Under pressure: the relationship between cranial shape and burrowing force in caecilians (Gymnophiona). Journal of Experimental Biology 224(18): 1–11. https://doi.org/10.1242/jeb.242964

Lowie A, De Kegel B, Wilkinson M, Measey J, O'Reilly JC, Kley NJ, Gaucher P, Brecko J, Kleinteich T, Herrel A, Adriaens D (2022) Regional differences in vertebral shape along the axial skeleton in caecilians (Amphibia: Gymnophiona). Journal of Anatomy: online early. https://doi.org/10.1111/joa.13682

Maddin HC (2011) Deciphering morphological variation in the braincase of caecilian amphibians (Gymnophiona). Journal of Morphology 272: 850–871. https://doi.org/10.1002/jmor.10953

Maddin HC, Russell AP, Anderson JS (2012) Phylogenetic implications of the morphology of the braincase of caecilian amphibians (Gymnophiona). Zoological Journal of the Linnean Society 166(1): 160–201. https://doi.org/10.1111/j.1096-3642.2012.00838.x

Marshall AF, Bardua C, Gower DJ, Wilkinson M, Sherratt E, Goswami A (2019) High-density three-dimensional morphometric analyses support conserved static (intraspecific) modularity in caecilian (Amphibia: Gymnophiona) crania. Biological Journal of the Linnean Society 126(4): 721–742. https://doi.org/10.1093/biolinnean/blz001

Müller H (2006) Ontogeny of the skull, lower jaw, and hyobranchial skeleton of *Hypogeophis rostratus* (Amphibia: Gymnophiona: Caeciliidae) revisited. Journal of Morphology, 267(8): 968–986. https://doi.org/10.1002/jmor.10454

Müller H, Oommen OV, Bartsch P (2005) Skeletal development of the direct-developing caecilian *Gegeneophis ramaswamii* (Amphibia: Gymnophiona: Caeciliidae). Zoomorphology 124: 171–188. https://doi.org/10.1007/s00435-005-0005-6

Norris HW, Hughes SP (1918) The cranial and anterior spinal nerves of the caecilian amphibians. Journal of Morphology 31: 489–560.

Nussbaum RA (1977) Rhinatrematidae: a new family of caecilians (Amphibia: Gymnophiona). Occasional Papers of the Museum of Zoology, University of Michigan 682: 1–30.

Nussbaum RA (1979) The taxonomic status of the caecilian genus *Uraeotyphlus* Peters. Occasional Papers of the Museum of Zoology, University of Michigan 687: 1–20.

Nussbaum RA (1983) The evolution of a unique dual jaw-closing mechanism in caecilians:(Amphibia: Gymnophiona) and its bearing on caecilian ancestry. Journal of Zoology 199(4): 545–554.

Nussbaum RA, Pfrender ME (1998) Revision of the African caecilian genus *Schistometopum* Parker (Amphibia: Gymnophiona: Caeciliidae). Miscellaneous Publications of the Museum of Zoology, University of Michigan 187: 1–32.

O'Reilly JC, Summers AP, Ritter DA (2000) The evolution of the functional role of trunk muscles during locomotion in adult amphibians. American Zoologist 40(1): 123–135. https://doi.org/10.1093/icb/40.1.123

Parker HW (1941) The Caecilians of the Seychelles. Annals and Magazine of Natural History 7(37): 1–17.

Peter K (1894) Die Wirbelsäule der Gymnophionen. Berichte der naturforschenden Gesellschaft zu Freiburg 9: 35–58.

Ramaswami LS (1941) Some aspects of the cranial morphology of *Uraeotyphlus narayani* Seshachar (Apoda). Records of the Indian Museum 43: 143–207.

Ramaswami LS (1942) An account of the head morphology of *Gegeneophis carnosus* (Beddome), Apoda. Journal of the Mysore University 3 (24): 205–220.

Ramaswami LS (1947) The chondrocranium of *Gegeneophis* (Apoda, Amphibia). Proceedings of the Zoological Society 118: 752–760.

Sarasin P, Sarasin F (1887–1890) Ergebnisse naturwissenschaftlicher Forschungen auf Ceylon in den Jahren 1884–1886 Band II: Zur Entwicklungsgeschichte und Anatomie der Ceylonesischen Blindwühle *Ichthyophis glutinosus*. Wiesbaden: C. W. Kreidels.

Schmidt A, Wake, MH (1990) Olfactory and vomeronasal systems of caecilians (Amphibia: Gymnophiona). Journal of Morphology 205(3): 255–268.

Sherratt E, Gower DJ, Klingenberg CP, Wilkinson M (2014) Evolution of cranial shape in caecilians (Amphibia: Gymnophiona). Evolutionary Biology 41: 528–545. https://doi.org/10.1007/s11692-014-9287-2

Straub JO (1985) Contributions to the cranial anatomy of the genus *Grandisonia* Taylor, 1968 (Amphibia: Gymnophiona). Inaugural dissertation, Universitat Basel, Switzerland.

Taylor EH (1964) A new species of caecilian from India (Amphibia, Gymnophiona). Senckenbergiana Biologica 45: 227–231.

Taylor EH (1968) The Caecilians of the World. A Taxonomic Review. University Kansas Press, Lawrence.

Taylor EH (1969) Skulls of Gymnophiona and their significance in the taxonomy of the group. The University of Kansas Science Bulletin 48 (15): 585–687.

Taylor EH (1970) On the Status of the caecilian *Indotyphlus battersbyi* Taylor. The University of Kansas Science Bulletin 49: 337–344.

Taylor EH (1977a) Comparative anatomy of caecilian anterior vertebrae. The University of Kansas Science Bulletin 51(6): 219–231.

Taylor EH (1977b) The comparative anatomy of caecilian mandibles and their teeth. The University of Kansas Science Bulletin 51(8): 261–282.

Theska T, Wilkinson M, Gower DJ, Müller H (2018) Musculoskeletal development of the Central African caecilian *Idiocranium russeli* (Amphibia: Gymnophiona: Indotyphlidae) and its bearing on the re-evolution of larvae in caecilian amphibians. Zoomorphology 138(1): 137–158. https://doi.org/10.1007/s00435-018-0420-0

Vitt LJ, Caldwell JP (2014) Herpetology, an Introductory Biology of Amphibians and Reptiles, 4th edition. Academic Press, London, UK.

Wake MH (1980) Morphometrics of the skeleton of *Dermophis mexicanus* (Amphibia Gymnophiona) Part I the vertebrae, with comparison to other species. Journal of Morphology 165: 17–130. https://doi.org/10.1002/jmor.1051650202

Wake MH (1986) The morphology of *ldiocranium russeli* (Amphibia: Gymnophiona), with comments on miniaturization through heterochrony. Journal of Morphology 189: 1–16. https://doi.org/10.1002/jmor.1051890102

Wake MH (1987) A new genus of African caecilian (Amphibia: Gymnophiona). Journal of Herpetology 21(1): 6–15. https://doi.org/10.2307/1564371

Wake MH (1993) Evolutionary diversification of cranial and spinal nerves and their targets in the gymnophione amphibians. Cells Tissues Organs 148: 160–168. https://doi.org/10.1159/000147535

Wake MH (2003) The osteology of caecilians. In: Heatwole H, Davies M (Eds) Amphibian Biology, Volume 5 Osteology. Chipping Norton, United Kingdom, 1809–1876.

Wake MH, Hanken J (1982) Development of the skull of *Dermophis mexicanus* (Amphibia: Gymnophiona), with comments on skull kinesis and amphibian relationships. Journal of Morphology 173: 203–223. https://doi.org/10.1002/jmor.1051730208

Wiedersheim R (1879) Die Anatomie der Gymnophionen. Jena: Gustav Fischer.

Wilkinson M (1992). Novel modification of the tetrapod cardiovascular system in the West African caecilian *Herpele squalostoma* (Amphibia: Gymnophiona: Caeciliidae). Journal of Zoology 228(2): 277–286. https://doi.org/10.1111/j.1469-7998.1992.tb04608.x

Wilkinson M, Mauro DS, Sherratt E, Gower DJ (2011) A nine-family classification of caecilians (Amphibia: Gymnophiona). Zootaxa 2874: 41–64. https://doi.org/10.11646/zootaxa.2874.1.3

Wilkinson M, Nussbaum RA (1997) Comparative morphology and evolution of the lungless caecilian *Atretochoana eiselti* (Taylor) (Amphibia: Gymnophiona: Typhlonectidae). Biological Journal of the Linnean Society 62: 39–109. https://doi.org/10.1111/j.1095-8312.1997.tb01616.x

Wilkinson M, Sherratt E, Starace F, Gower DJ (2013) A new species of skin-feeding caecilian and the first report of reproductive mode in *Microcaecilia* (Amphibia: Gymnophiona: Siphonopidae). PLoS One 8(3): e57756. https://doi.org/10.1371/journal.pone.0057756